Soft Matter

ROYAL SOCIETY OF CHEMISTRY

PAPER

View Article Online
View Journal | View Issue

Cite this: *Soft Matter*, 2022, **18**, 7360

Preparation of a novel regenerated silk fibroin-based hydrogel for extrusion bioprinting†

Ni Chen,[a] Xinbo Zhang,[b] Jinyang Lyu,[c] Guanglei Zhao,[c] Kai Gu,[a] Jun Xia,[c] Zhongchun Chen[d] and Zhengzhong Shao*[a]

Three-dimensional (3D) bioprinting technology, allowing rapid prototyping and personalized customization, has received much attention in recent years, while regenerated silk fibroin (RSF) has also been widely investigated for its excellent biocompatibility, processibility, and comprehensive mechanical properties. However, due to the difficulty in curing RSF aqueous solution and the tendency of conformational transition of RSF chains under shearing, it is rather complicated to fabricate RSF-based materials with high mechanical strength through extrusion bioprinting. To solve this problem, a printable hydrogel with thixotropy was prepared from regenerated silk fibroin with high-molecular-weight (HMWRSF) combined with a small amount of hydroxypropyl methylcellulose (HPMC) in urea containing aqueous solution. It was found that the introduction of urea could not only vary the solid content of the hydrogel to benefit the mechanical properties of the 3D-bioprinted pre-cured hydrogels or 3D-bioprinted sponges, but also expand the "printable window" of this system. Indeed, the printability and rheological properties could be modulated by varying the solid content, the heating time, the urea/HMWRSF weight ratio, *etc.* Moreover, the microstructure of nanospheres stacked in these lyophilized 3D-bioprinted sponges was interesting to observe, which indicated the existence of microhydrogels and both "the reversible network" and "the irreversible network" in this HMWRSF-based pre-cured hydrogel. Like other HMWRSF materials fabricated in other ways, these 3D-bioprinted HMWRSF-based sponges exhibited good cytocompatibility for dental pulp mesenchymal stem cells. This work may inspire the design of functional HMWRSF-based materials by regulating the relationship between structure and properties.

Received 22nd July 2022,
Accepted 24th August 2022

DOI: 10.1039/d2sm00984f

rsc.li/soft-matter-journal

1. Introduction

Three-dimensional (3D) bioprinting is transforming the landscape of traditional manufacturing and is becoming an effective and versatile method for biomedical and clinical applications.[1–4] Precision medicine benefits from 3D bioprinting because it allows for quick prototyping of tailored structure and morphology with the needed components. In terms of regulating the intricate spatial arrangement of diverse components to duplicate the heterogeneity of original tissue, 3D bioprinting has an advantage over traditional production. By managing the structure–property relationship, 3D bioprinting also allows manipulation of many properties of obtained materials, such as mechanical attributes, degradation rate, *etc.*

Generally, 3D bioprinting approaches can be classified into three main categories including material jetting,[5,6] material extrusion,[7–9] and vat polymerization.[10–12] Among these three approaches, material jetting, especially drop-on-demand inkjet bioprinting, is attractive for contactless deposition and patterning of different types of living cells or even a single cell with biomaterials.[13] Vat polymerization is an emerging biofabrication method due to its printing accuracy and resolution in the nanoscale region (~100 nm).[14,15] Nevertheless, material extrusion (or extrusion-based 3D bioprinting) is the most prevalent technique for its compatibility with a wide range of printable biomaterials, ease of preparation, and fast fabrication speed.[16] In the extrusion-based 3D bioprinting process, the bioink performs a crucial role as its rheological properties, biochemical characteristics, and material traits significantly affect the printability and functionality of 3D bioprinting.[17–19] A wide variety of materials have been developed for extrusion-based bioprinting inks, including ceramics,[20] glass,[21] synthetic polymers,[22] and natural polymers.[23,24] Proteins are important components of cells, extracellular matrix, and a variety

[a] *State Key Laboratory of Molecular Engineering of Polymers, Laboratory of Advanced Materials and Department of Macromolecular Science, Fudan University, Shanghai 200433, P. R. China. E-mail: zzshao@fudan.edu.cn*
[b] *Department of Materials Science and Engineering, Southern University of Science and Technology, Shenzhen, Guangdong 518055, P. R. China*
[c] *Department of Orthopedic Surgery, Huashan Hospital, Fudan University, Shanghai 200040, P. R. China*
[d] *Department of Otorhinolaryngology-Head and Neck Surgery, Huashan Hospital, Fudan University, Shanghai 200040, P. R. China*

† Electronic supplementary information (ESI) available. See DOI: https://doi.org/10.1039/d2sm00984f

of biological structures, and therefore protein-based inks are expected to reduce immune reactions and aid material and host integration. Furthermore, they gradually degrade over time, yielding peptides and amino acids that can be utilized as nutrients in the body.[25]

As an abundant natural protein, regenerated silk fibroin (RSF) extracted from *Bombyx mori* silkworm silk has very good processability and can be prepared into a variety of materials with different traits, including membranes, microspheres, fibers, hydrogels, scaffolds, *etc.*[26–30] Due to their good biocompatibility, excellent processability, and comprehensive mechanical properties, RSF-based materials have also attracted the attention of researchers in the field of 3D bioprinting. For example, a simple method is to directly deposit high-concentration RSF aqueous solution (28–30 wt%) into 86% methanol aqueous solution and the obtained scaffold had good biocompatibility and supported the adhesion and growth of human mesenchymal stem cells (hMSCs).[31] However, during the printing process, the strong shear force generated at the nozzle and polar solvent of methanol would rapidly induce the conformational transition of the RSF chain from a random coil to β-sheet. Even though β-sheet is a secondary structure, it could further develop into β-sheet microcrystals, large β-sheet crystal aggregates or even macroscopic RSF microfibers and their aggregates, which may clog the nozzle.[32] In addition, this direct writing process also causes the 3D-bioprinted material with poor mechanical properties. To solve this problem, scholars improved the printability of RSF by blending with other components such as gelatin with temperature-dependent gelation behaviour, while glycerol was added to promote physical cross-linking.[33] However, the introduction of a large amount of gelatin leads to a low elastic modulus of the 3D-bioprinted hydrogel, which does not demonstrate the excellent comprehensive mechanical properties of RSF, limiting the application of the material. In this case, our previous work has successfully applied the RSF microhydrogel with thixotropy to extrusion printing.[34] Due to the presence of a relatively high β-sheet domain content in the hydrogel, the 3D-bioprinted hydrogel possesses remarkable mechanical properties. Nevertheless, in order to ensure its self-supporting performance during the printing procedure, the solid content of the hydrogel should be relatively high (20–30 wt%) because of the relatively low molecular weight of regenerated silk fibroin (around 95 kDa) employed, which may limit 3D culture of cells in this hydrogel, resulting in decreased cell viability.[35] Therefore, it is essential to fabricate a 3D-bioprinted RSF material with both good mechanical properties and a lower solid content.

It was reported that a high-molecular-weight regenerated silk fibroin/hydroxypropyl methylcellulose (HMWRSF/HPMC) mixed solution could form a hydrogel with excellent mechanical properties at 70 °C, and the compressive modulus and tensile modulus of a 10 wt% HMWRSF/HPMC hydrogel could both exceed 1.0 MPa, which outweighed hydrogels fabricated using other biomacromolecules.[36]

It is well known that the properties of RSF-based materials are largely dependent on their molecular weight and processing techniques. In this work, we tried to prepare a HMWRSF/HPMC hydrogel with thixotropy and expect that it could be directly printed into designed models, and the obtained 3D-bioprinted materials with excellent compressive modulus and strength could find potential application in tissue engineering. We hypothesized that urea was able to work as a hydrogen bond disturber to affect the gelation process of the HMWRSF/HPMC mixed solution upon heating at 70 °C. Aside from the printability and rheological properties of such printable hydrogels, the mechanical properties of 3D-bioprinted materials were investigated in detail. The microscopic morphology of the samples obtained after freezing–ripening–thawing–lyophilizing the printable hydrogel was observed. Based on the above, the relationship between the regulation of the hydrogel structure and its performance in the whole fabrication process was also discussed.

2. Experimental section

2.1 Materials

High-molecular-weight regenerated silk fibroin (HMWRSF) aqueous solution and low-molecular-weight regenerated silk fibroin (LMWRSF) aqueous solution were prepared by degumming and dissolving of *Bombyx mori* silkworm silk according to the established steps with some modifications.[37] Silk cocoons (purchased from Jiangsu Province, China) were boiled in 0.5 wt% $NaHCO_3$ aqueous solution or 0.5 wt% Na_2CO_3 aqueous solution to remove sericin. These two kinds of degummed silks were separately dissolved in 9.3 mol L^{-1} of LiBr aqueous solution at 60 °C in a water bath for an hour. After being filtered by a gauze of eight layers, the HMWRSF aqueous solution with a molecular weight of 150–180 kDa and the LMWRSF aqueous solution with a molecular weight of around 95 000 Da were dialyzed against deionized water for 3 days at room temperature by using a 12–14 kDa cutoff semipermeable membrane, respectively. The dialyzed HMWRSF aqueous solution or LMWRSF aqueous solution was then clarified by centrifugation at 8911 × *g* for 10 minutes. The supernatant, which was HMWRSF aqueous solution or LMWRSF aqueous solution with a concentration of around 4% (w/w), was concentrated against PEG solution to above 10 wt%.

Hydroxypropyl methylcellulose (HPMC) with the degree of substitution (DS) of the hydroxypropyl group of 7.0–12% and the DS of the methoxy group of 28–30% was purchased from Aladdin Co. Ltd, Shanghai, China. The viscosity of the 2 wt% HPMC aqueous solution was 6 mPa s. A 10 wt% HPMC aqueous solution was prepared by dissolving HPMC in deionized water. The preparation procedure of all the samples investigated in this work is depicted in Fig. 1.

2.2 Preparation of HMWRSF-based pre-cured hydrogels and LMWRSF-based pre-cured hydrogels

It is well known that it takes a couple of days for the RSF aqueous solution to form a hydrogel spontaneously while a small amount of HPMC could promote RSF chain conformational transition and gelation within a few minutes upon heating, according to our previous work.[36] Although the RSF

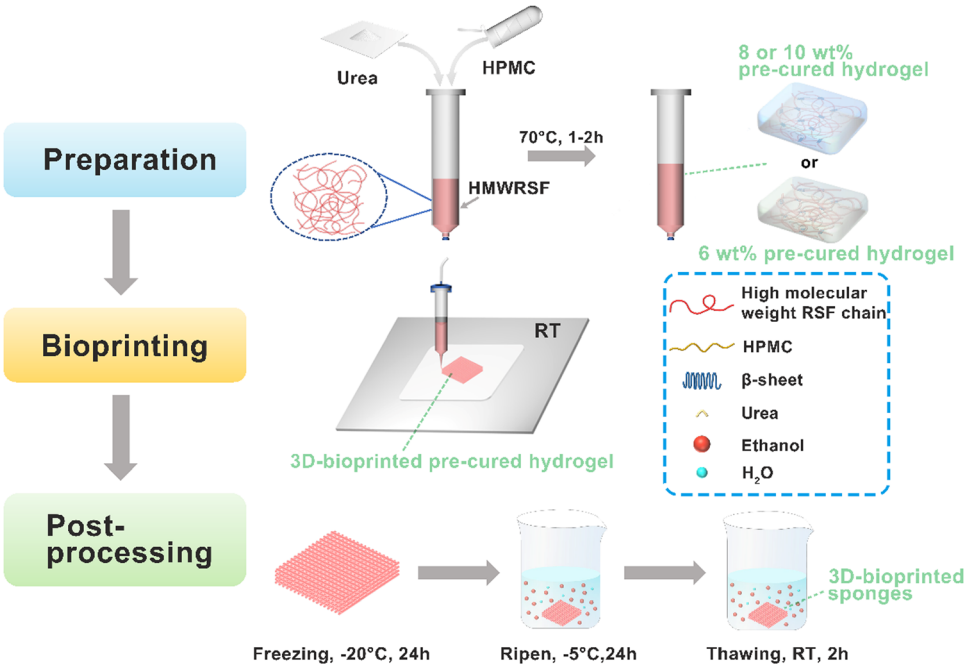

Fig. 1 Schematic illustration of the preparation, bioprinting, and post-processing procedure of HMWRSF-based pre-cured hydrogels. HMWRSF: high-molecular-weight regenerated silk fibroin, HPMC: hydroxypropyl methylcellulose, and RT: room temperature. Urea was not introduced for a 6 wt% pre-cured hydrogel.

with high molecular weight, increasing solid content or heating time, *etc.* could facilitate the formation of the RSF/HPMC hydrogel with high mechanical strength, it was unfeasible for 3D-bioprinting. The present work was aimed at preparing HMWRSF/HPMC with thixotropy, which could be directly 3D-bioprinted, and the ripened 3D-bioprinted HMWRSF material shows significant mechanical properties.

In a series of pre-experiments, we found that the HMWRSF/HPMC pre-cured hydrogel with a solid content less than 6 wt% could not stand free after being extruded, because the low concentration of HMWRSF resulted in insufficient physical crosslinks and then low mechanical strength. Increasing the heating time did not facilitate the preparation of a printable hydrogel. However, the 6 wt% HMWRSF/HPMC pre-cured hydrogel showed good thixotropy and printability upon controlling the heating time of the HMWRSF/HPMC aqueous solution, because a relatively high solid content caused suitable mechanical strength, which made sure flow extrusion and sufficient self-supporting ability. Upon increasing the solid content to 8 wt% or 10 wt%, the mechanical strength of the hydrogel was relatively high but the heavy extrusion swelling or impossibility of extrusion occurred. In this case, the introduction of urea as a hydrogen bond disturber is necessary because it may prolong the gelation process of the HMWRSF/HPMC hydrogel and regulate the mechanical properties of the HMWRSF/HPMC pre-cured hydrogel. Thereby, urea may endow the pre-cured hydrogels of a high solid content with thixotropy and printability. More importantly, the soluble urea could be removed thoroughly from the ripened 3D-bioprinted HMWRSF material. The following is the specific discussion for preparing printable HMWRSF-based pre-cured hydrogels.

In particular, HMWRSF aqueous solution with various concentrations was mixed with the HPMC aqueous solution and the optimal weight ratio of HMWRSF to HPMC was maintained at 9 : 1. Three HMWRSF-based pre-cured hydrogels for each solid content were chosen: one ink lacking printability due to poor self-standing ability, one with good printability, and one which lacks printability due to strong physical crosslinking. For the samples with a solid content of 6 wt%, the mixed solutions were heated at 70 °C for 1, 1.5, and 2 hours, respectively, to produce three different HMWRSF-based pre-cured hydrogels, named 6%-0-1h, 6%-0-1.5h, and 6%-0-2h, with respect to their solid content, urea content, and heating time. For samples with solid contents of 8 wt% and 10 wt%, urea was introduced to the HMWRSF/HPMC mixed solution. The weight ratio of urea to HMWRSF was 0.3, 0.5, and 0.7 in the 8 wt% HMWRSF/HPMC solution while it was 0.8, 1.0, and 1.2 in the 10 wt% HMWRSF/HPMC solution, respectively. These mixed solutions were heated at 70 °C for 1 hour to produce HMWRSF-based pre-cured hydrogels, and the pre-cured hydrogels were named 8%-0.3-1h, 8%-0.5-1h, 8%-0.7-1h, 10%-0.8-1h, 10%-1.0-1h, and 10%-1.2-1h, respectively.

In addition, LMWRSF-based pre-cured hydrogels were prepared. The weight ratio of LMWRSF to HPMC remained at 9 : 1 and the uniformly mixed LMWRSF/HPMC solution with different solid contents was heated at 70 °C for 1 hour to obtain LMWRSF-based pre-cured hydrogels.

2.3 Rheological measurements

A rheological test was conducted on a Physica MCR301 rheometer (Anton Paar, Austria) using a parallel plate of 25 mm diameter. In order to prevent water evaporation during the test,

a thin paraffin layer was applied to the edge of the sample. Amplitude sweep of the 6%-0-1h pre-cured hydrogel was performed and the linear viscoelastic region (LVE) was obtained. To monitor the gelation process of the HMWRSF-based pre-cured hydrogels, the oscillation mode was applied to the samples named s-10%-0-1h and s-10%-1.0-1h (''s'' represents solution) with a fixed frequency of 1 Hz, an amplitude of 1% and a temperature of 70 °C. It was worth mentioning that all samples were loaded on the plate at 25 °C and equilibrated for 5 minutes. The sample was heated at a rate of 0.5 °C s^{-1} from 25 °C to 70 °C and the temperature was kept at 70 °C during the measurement. To investigate the structural destruction and recovery, the oscillation mode was used in the 3-interval thixotropy test (3ITT) with a frequency of 1 Hz at 25 °C, a large amplitude of 500% for 200 s during the structural destruction stage and a small amplitude of 1% for 100 s during the structural recovery stage.

2.4 Bioprinting and production of 3D-bioprinted sponges

The HMWRSF-based pre-cured hydrogels and the LMWRSF-based pre-cured hydrogels which were directly prepared in a barrel were extruded using a 3D-bioprinter (Regenovo, China) with a 0.34 mm straight needle at room temperature. The air pressure was adjusted between 0.15 and 0.3 MPa and the printing speed was 40 mm s^{-1}. The 3D bioprinting models were converted to the STL format and the filling interval was maintained at 0 mm or 2 mm. To visualize the printability, these HMWRSF-based pre-cured hydrogels with various cross-linking degrees were printed into parallel strands by setting the printing parameters. Afterwards, multilayered HMWRSF-based and LMWRSF-based 3D-bioprinted pre-cured hydrogels were prepared and they were also post-processed according to the published work[38] to obtain HMWRSF-based 3D-bioprinted sponges named r-6%-0-2h, r-8%-0.5-1h, and r-10%-1.0-1h, respectively, for the following characterization (''r-6%-0-2h'' refers to a ripened 3D-bioprinted sponge, the corresponding pre-cured hydrogel of which was named ''6%-0-2h'') and LMWRSF-based 3D-bioprinted sponges named r-L-6%-0-1h, r-L-8%-0-1h, and r-L-10%-0-1h, representing ripened sponges, low-molecular-weight, solid content of pre-cured hydrogels, urea content and the heating time, respectively. Generally, post-processing was that the 3D-bioprinted pre-cured hydrogels were frozen at −20 °C for 24 hours and then ripened in ethanol at −5 °C for 24 hours and thawed at room temperature for 2 hours. The obtained HMWRSF-based 3D-bioprinted sponges were dialyzed against deionized water for 3 days at room temperature to remove urea and ethanol thoroughly.

2.5 Mechanical properties testing

The compression test was carried out on an Instron 5966 with a 500 N sensor at a compression rate of 1 mm min^{-1}. Due to the very low mechanical strength, the r-L-6%-0-1h sample could not be applied for the compression test. The cuboid HMWRSF-based 3D-bioprinted sponges (r-6%-0-2h, r-8%-0.5-1h, and r-10%-1.0-1h) and LMWRSF-based 3D-bioprinted sponges (r-L-8%-0-1h and r-L-10%-0-1h) with a length and width of 5 mm, respectively, and a height of 9 mm were used for measurements. The filling interval of all the 3D-bioprinted sponges used for compression tests was 0 mm and their apparent density (D_a) was calculated using the formula of ''D_a (mg mm^{-3}) = weight of the 3D-bioprinted sponge/volume of the 3D-bioprinted sponge''.

To detect the influence of urea on the mechanical strength of HMWRSF-based materials, HMWRSF-based hydrogels with or without urea were prepared according to our published work.[36] During the process of ripening in 75% ethanol and dialysis against deionized water, urea from the HMWRSF-based hydrogels was able to be removed thoroughly. The cylindrical ripened hydrogels with various solid contents prepared with a diameter of 10 mm and a height of 10 mm were used for compression measurement at the same compression rate of 1 mm min^{-1}. The samples of ripened hydrogels were named r-6%-0, r-8%-0, r-10%-0, r-6%-0.2, r-8%-0.5, and r-10%-1.0, representing the ripened hydrogel, solid content, and the weight ratio of urea to HMWRSF, respectively. Due to the change in the solid content of the hydrogel after ripening in 75% ethanol, the actual solid content of these ripened hydrogels was calculated using the formula: W_a (%) = (W_d/W_h) × 100%, where W_a is the actual solid content, W_d is the weight of the dried hydrogel, and W_h is the weight of the hydrogel.

2.6 Morphological observation of the lyophilized samples

Four sponges were obtained by freezing the four samples including the HMWRSF-based mixed solution, HMWRSF-based pre-cured hydrogels (different stages) and ripened HMWRSF-based hydrogel at −20 °C for 24 hours, then placed in ethanol at −5 °C for 24 hours and eventually thawed at room temperature for 2 hours. The cross-sectional morphologies of the lyophilized samples from the four sponges were observed using a Hitachi S-4800 (Hitachi, Japan) field emission scanning electron microscope (FE-SEM) at 1 kV. These samples were gold-coated for 60 s before being observed.

2.7 Attenuated total reflection Fourier transform infrared (ATR-FTIR) characterization

The spectra of the three lyophilized samples r-6%-0, r-6%-0-0h and r-6%-0-2h, which were the ripened HMWRSF-based hydrogel, HMWRSF-based solution, and HMWRSF-based pre-cured hydrogel, respectively, were obtained using an attenuated total reflectance Fourier transform infrared spectrometer (ATR-FTIR, Nicolet 6700, USA) in the range of 1350–1900 cm^{-1} with 64 scans and 4.0 cm^{-1} resolution.

2.8 Cell culture and viability

Dental pulp mesenchymal stem cells (DPSCs, gifted by Utooth Biological Technology Co., Ltd, Zhejiang, China) were cultured in α-MEM supplemented with 10% fetal bovine serum and 1% penicillin–streptomycin under 5% CO_2 and 37 °C. After removing urea and ethanol completely, the HMWRSF/HPMC scaffolds *via* bioprinting were immersed in a complete medium and fully soaked. DPSCs were detached from cell culture flasks with trypsin and were resuspended in a fresh complete medium at a

concentration of 2×10^7 cells per mL. 100 μL of the cell suspension was pipetted onto the surface of the scaffolds. After incubation for 2 h to adhere the cells, 1 mL of the α-MEM complete medium was added and then the scaffolds with cells were placed in an incubator for continuous culture, and the complete medium was changed every 2 days. The cell viability on the 3D-bioprinted scaffolds was assessed by the cell counting kit-8 (CCK-8) assay. Briefly, the cell-laden scaffolds were transferred to a new 48-well plate on the 1st day, 3rd day, 5th day, and 7th day, respectively. 0.11 mL of 10% CCK-8 DMEM solution was added to each well and incubated for 2 h. Afterwards, 100 μL of the reaction solution was transferred to a 96-well plate, and the optical density was detected on a microplate reader (BioTek, USA) at 450 nm.

3. Results and discussion

3.1 Rheology of HMWRSF-based pre-cured hydrogels

The 3-interval thixotropy test (3ITT) was applied to the HMWRSF-based pre-cured hydrogels of various solid contents or urea contents to investigate their thixotropy, as shown in Fig. 2 and Fig. S1 (ESI†). Reasonably, G' is higher than G'' in the first stage of the small amplitude oscillatory shear (SAOS) test with a 1% amplitude as the sample was in a hydrogel state, while G' dramatically decreased and was far lower than G'' in the second stage of the large amplitude oscillatory shear (LAOS) test with a 500% amplitude as the sample exhibited fluidity. During the third stage when applying the SAOS test with a 1% amplitude once again, G' increased sharply, higher than G'' again, and the recovery process could be completed within a very short time. It is worth mentioning that the rheological behaviour of the HMWRSF-based pre-cured hydrogel during the first cycle of the 3ITT test slightly differs from those in the following cycles because of its irreversible interactions which could be destroyed permanently when the large shear force was employed.[39] Therefore, these HMWRSF-based pre-cured hydrogels have thixotropy but they are not very representative thixotropic materials.

Although all the HMWRSF-based pre-cured hydrogels presented thixotropy to some extent, the pre-cured hydrogel with both shear-thinning and sufficient self-standing features was considered to be a suitable ink for extrusion bioprinting. In this work, the printability of the pre-cured hydrogel can be controlled by regulating many factors, including the solid content, the heating time of HMWRSF-based mixed solution and the urea content. Generally, in terms of lower solid contents such as 6 wt% (Fig. 2(A)), the longer heating time duration corresponds to a higher storage modulus, which is demanded as more physical crosslinking could be formed for better printability. In terms of higher solid contents such as 8 wt% (Fig. 2(B)) or 10 wt% (Fig. 2(C)), the addition of urea was necessary, and more urea resulted in a lower G' modulus because urea may prolong the formation of β-sheet microcrystals[40,41] and allow the pre-cured hydrogel to be extruded fluently from the narrow nozzle. Therefore, the pre-cured hydrogels of 6%-0-2h, 8%-0.5-1h and 10%-1.0-1h that are both shear-thinned and sufficiently self-stood were regarded as the suitable raw materials for being 3D-bioprinted.

The reversible behaviour of structural breakdown recovery may be attributed to reversible interactions in our pre-cured hydrogels. Our previous work[34] proposed that the printable RSF hydrogel was a RSF microhydrogel in essence and there were abundant reversible interactions including hydrophobic interactions, entanglement, even a few undefined hydrogen bonds, *etc.* among the outer peripheral areas of the RSF microhydrogel, contributing to its thixotropy and printability. Likewise, regulating factors such as the solid content, the heating time of HMWRSF-based mixed solution and the urea content allowed us to balance the ratio of the irreversible RSF microhydrogel aggregates and the reversible interaction in the formulation to obtain a suitable ink (pre-cured/printable hydrogel) for extrusion-based bioprinting. The later part would further explain the role urea played in the whole extrusion-based bioprinting.

3.2 Printability of HMWRSF-based pre-cured hydrogels

Accordingly, the following serves to further visualize the influence of these factors on the rheological behaviour and further on the printability of the pre-cured hydrogel. When looking at the parallel strands from the formulations of 6%-0-1h (Fig. 3A(a)), 6%-0-1.5 h (Fig. 3A(b)), and 8%-0.7-1h (Fig. 3A(f)), a lack of shape fidelity can be clearly observed due to the lower storage modulus and poor self-standing ability. However, the parallel strands from the formulations of 8%-0.3-1h (Fig. 3(d)) and 10%-0.8-1h (Fig. 3A(g)) demonstrate obviously an extrusion swelling phenomenon due to higher storage modulus. In contrast to the

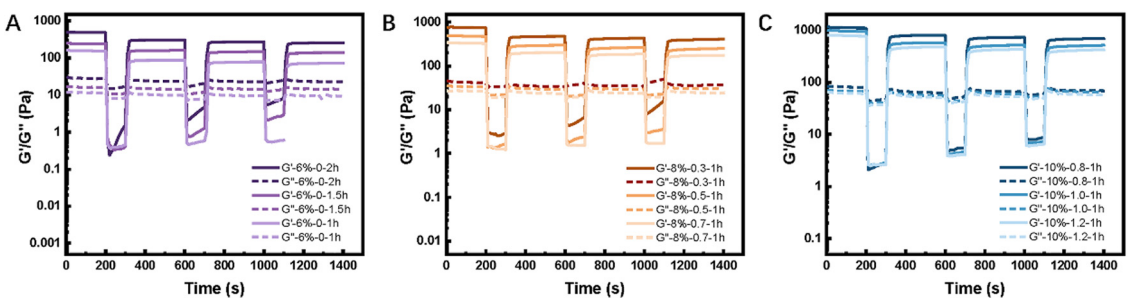

Fig. 2 Destruction recovery test of HMWRSF-based pre-cured hydrogels with different solid contents, (A) 6%, (B) 8%, and (C) 10%, and varying urea contents or heat times at 25 °C.

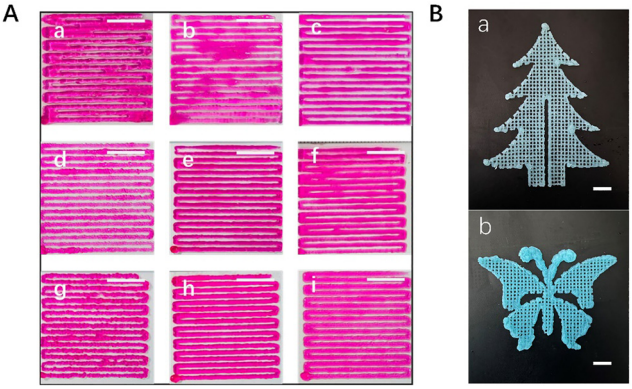

Fig. 3 Digital images of 3D-bioprinted (A) parallel strands of pre-cured hydrogels, a.b-6%-0-1h, b.b-6%-0-1.5 h, c.b-6%-0-2h, d.b-8%-0.3-1h, e.b-8%-0.5-1h, f.b-8%-0.7-1h, g.b-10%-0.8-1h, h.b-10%-1.0-1h, and i.b-10%-1.2-1h, "b" refers to "3D-bioprinted", and (B) multi-layered complex structures in a tree shape (a) and a butterfly shape (b). The scale bar is 1 cm.

formulations above, the 6%-0-2h (Fig. 3A(c)), 8%-0.5-1h (Fig. 3A(e)), and 10%-1.0-1h (Fig. 3A(h)) pre-cured hydrogels possessed both good shape fidelity and flow extrusion. To further emphasize the printability and shape fidelity of the excellent ink, more complex designed structures in "tree" shape (Fig. 3B(a)) and in "butterfly" shape (Fig. 3B(b)) with four layers were printed using the 10%-1.0-1h pre-cured hydrogel. To sum up, considering the good printability, these three pre-cured hydrogels, the 6%-0-2h, the 8%-0.5-1h, and the 10%-1.0-1h pre-cured hydrogels, were applied to be 3D-bioprinted and the properties of HMWRSF-based 3D-bioprinted materials were further studied.

3.3 Mechanical characterization of 3D-bioprinted HMWRSF-based sponges

As we all know, it is hard to be applied to an actual scenario such as bone regeneration for materials with poor mechanical properties. However, the HMWRSF-based pre-cured hydrogel was able to gain great improvement in mechanical behaviour

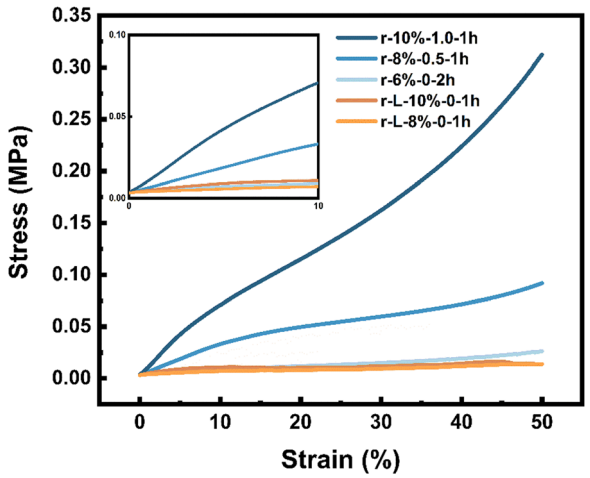

Fig. 4 Compressive stress–strain curves of 3D-bioprinted HMWRSF and LMWRSF hydrogel-based sponges. Inset: Compressive stress curves of the first 10% strain.

Table 1 Apparent density and compression modulus of various 3D-bioprinted RSF hydrogel-based scaffolds, n = 5

Samples	Apparent density (mg mm^{-3})	Compressive modulus (MPa)
r-10%-1.0-1h	0.96 ± 0.12	0.88 ± 0.11
r-8%-0.5-1h	0.80 ± 0.02	0.34 ± 0.10
r-6%-0-2h	0.55 ± 0.03	0.068 ± 0.014
r-L-10%-0-1h	0.55 ± 0.02	0.12 ± 0.01
r-L-8%-0-1h	0.47 ± 0.04	0.035 ± 0.010

after ripening in 75% ethanol because of the irreversible physical crosslinking network of a well-defined β-sheet domain formed.[42–44] It is also reported that the HMWRSF scaffold is beneficial for cell adhesion and 3D culture.[45,46] In this case, 3D-bioprinted HMWRSF sponges with significant mechanical properties were prepared.

To investigate the mechanical properties, compression tests on 3D-bioprinted HMWRSF-based sponges were conducted (Fig. 4). Unsurprisingly, the compression modulus highly corresponded to the solid content of the pre-cured hydrogel and the apparent density of the scaffold; the higher the solid content and the apparent density, the stronger the 3D-bioprinted HMWRSF-based sponges. It should also be noted that the compressive modulus of the 3D-bioprinted HMWRSF-based sponges could be adjusted from around 0.07 MPa to 0.9 MPa (Table 1). In contrast, the as-prepared scaffolds prepared using low-molecular-weight (LMW) RSF possessed lower apparent density and lower compressive modulus although their solid contents of pre-cured hydrogels were the same. What is more, Fig. S2 (ESI†) shows that HMWRSF hydrogel-based scaffolds had much better compression strength since their compressive strain to break was over 50%. Therefore, the 3D-bioprinted HMWRSF-based sponges might be applied for human articular cartilage regeneration due to their good mechanical properties.[47,48]

3.4 Influence of urea on the extrusion-based bioprinting process

As mentioned above, urea as a hydrogen bond disturber may prolong the formation of HMWRSF β-sheet microcrystals and further prolong the gelation point. This is because the cross-linker in the HMWRSF physical hydrogel was the β-sheet microcrystal/domain whose formation is on account of that hydrogen bonds as driving force induce the RSF molecular chains to organize. The following experiment also proves this hypothesis. Rheological experiments of homogeneous HMWRSF/HPMC solutions with various solid contents and urea contents were carried out at 70 °C to evaluate the storage modulus (G') and the loss modulus (G'') (Fig. S3, ESI†). As we expected, without the addition of urea, a homogeneous 10 wt% HMWRSF/HPMC solution could form a hydrogel very quickly upon heating at 70 °C, the gelation point of which was hardly observed in a rotational rheometer. In terms of a homogeneous HMWRSF/HPMC/urea solution with a solid content of 10 wt%, whose corresponding urea/HMWRSF weight ratio was 1.0, a gelation point could be found, indicating that the postponed gelation was caused by the addition of urea.

In our previous work,[36] we found that HPMC could promote HMWRSF conformational transition into a β-sheet domain upon heating at 70 °C very quickly and the HMWRSF/HPMC hydrogel with a relatively high solid content is not feasible for 3D printing or being injected. In our case, urea was added and could endow the HMWRSF/HPMC hydrogel with the printable property. Actually, based on the conclusion above, it is easy to know that there is a "trade-off" between urea and HPMC, which both affect the gelation process of the RSF/HPMC hydrogel and endow it with printability.

To investigate the effect of urea on the final mechanical properties, RSF/HPMC hydrogels with or without urea were prepared and then measured using the compression test (Fig. S4, ESI†). Considering both the solid content and the compressive modulus, there was no obvious difference in mechanical properties between the hydrogels with or without urea (Table S1, ESI†), which was in agreement with our expectation, that is, urea prolonged the formation of β-sheet microcrystals as well as the gelation process as a hydrogen bond disturber, but had little effect on the mechanical properties of the material.

3.5 Microscopic morphologies of lyophilized HMWRSF microhydrogel sponges and HMWRSF hydrogel sponges

After lyophilizing, the microscopic morphologies of these sponges from HMWRSF aqueous solution and its hydrogel in different stages are presented in Fig. 5. It can be found that no matter whether lyophilized from the 6% HMWRSF/HPMC aqueous solution-based sponges or from its pre-cured hydrogel-based sponges, the cross-sections of both samples were dominated by the wall of aggregated nanospheres (Fig. 5(A2) and (B2)). Further gelation would leave the plate wall with the trace of nanospheres in the lyophilized microhydrogel-based sponges (Fig. 5(C2)), suggesting the possible fusion of nanospheres. After ripening in ethanol, the wall turned to nearly plate in the lyophilized hydrogel-based sponges (Fig. 5(D2)). It was worth noting that such microscopic morphologies developed during the gelation process would not be changed too much by the involvement of urea, as the ones of 8%-0.5 (*i.e.* aqueous solution of 8% HMWRSF/HPMC with urea, the weight ratio of urea to HMWRSF was 0.5) and 10%-1.0 presented a very similar morphology to their counterparts of 6% HMWRSF/HPMC (Fig. S5 and S6, ESI†).

Previously, it was reported that the HMWRSF microspheres could be produced by freezing a lower concentrated aqueous solution of HMWRSF (1–8 mg mL^{-1}) with a certain amount of ethanol, because ethanol induced β-sheet nuclei to develop into β-sheet microcrystals and the shear force caused by ice formation and growth could result in mature β-sheet dominated microspheres which were isolated by formed ice.[49] On the other hand, it was found that HPMC played a role to promote the conformational transition of HMWRSF, and heating could accelerate this transition to develop β-sheet crystallite domains.[36] In our case, after freezing the samples at the early stage of gelation, *e.g.* the solution or pre-cured hydrogel, the HMWRSF preferred to be nanospheres, because HPMC acted as a promotor of the RSF β-sheet domain to induce the formation of the RSF microhydrogel (*i.e.* RSF β-sheet microcrystals) and the shear force caused by ice formation and growth was able to make these RSF microhydrogel transform into RSF nanospheres. It should be noted that the presence of microhydrogel was crucial for the printability of RSF-based hydrogels.[34] However, due to the relatively high solid content of the solution or pre-cured hydrogel, the amount of RSF microhydrogel was high accordingly and the nanospheres originated from RSF microhydrogel were prone to accumulate to each other. In terms of the samples lyophilized from the ripened hydrogel, normal morphologies such as plate walls and nanofibrils were observed. This is because the network in the HMWRSF/HPMC hydrogel was sufficiently developed while those small and evenly distributed HMWRSF microcrystals served as physical crosslinkers at the late stage of gelation.

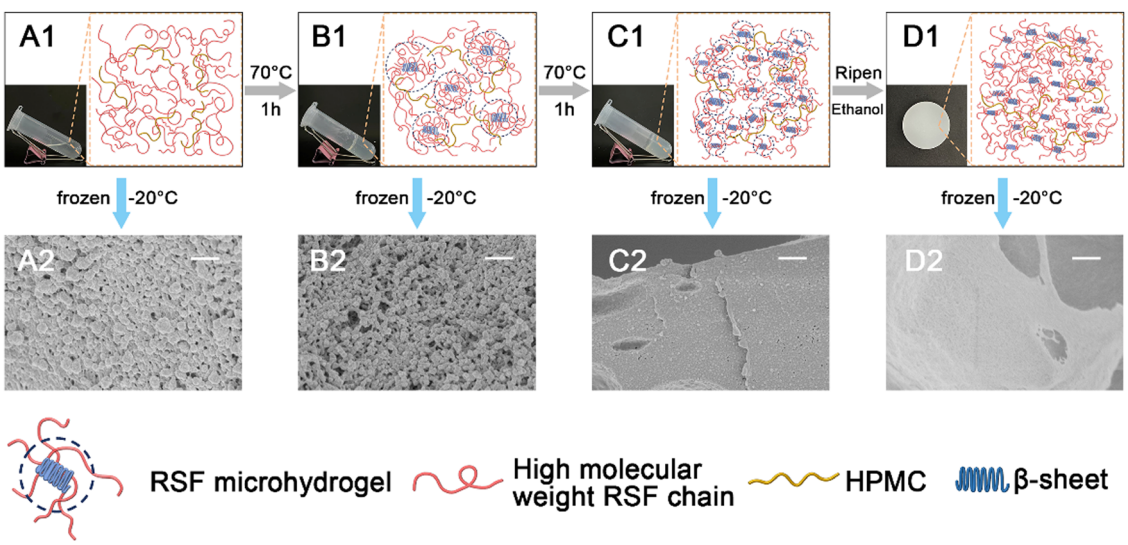

Fig. 5 Digital images and schemes of molecule chain in 6% HMWRSF/HPMC aqueous solution (A1) and its produced hydrogel at different stages (B1)–(D1). SEM images of the cross-section of those corresponding samples after lyophilization (A2)–(D2). The scale bar is 500 nm.

It could be seen in the digital pictures in Fig. 5 that the transmittance of the samples gradually decreased during the gelation process and the ripened hydrogel turned opaque eventually. It suggested the growth of the β-sheet domain, which could be demonstrated by ATR-FTIR characterization. As shown in Fig. S7 (ESI†), the peak around 1623 cm^{-1} which was assigned to amide I of the RSF β-sheet structure[50] became narrow and sharp in the r-6% sample, indicating the increase of the β-sheet structure.

3.6 *In vitro* cell proliferation on bioprinted HMWRSF-based scaffolds

The good biocompatibility of the RSF-based material has been widely reported in the literature.[51] To verify that our 3D-bioprinted HMWRSF-based scaffolds are also capable of supporting cell growth and proliferation, dental pulp mesenchymal stem cells (DPSCs) were seeded onto the bioprinted HMWRSF-based scaffold grid with the size of 0.8 mm and various solid contents. As shown in Fig. S8 (ESI†), DPSCs remain viable and proliferate significantly on the three scaffolds over 7 days, indicating the excellent cytocompatibility of the material. In our case, the proliferation of the cells is significantly related to the apparent density of the materials and DPSCs prefer the HMWRSF-based scaffolds with lower density, which may be due to the larger and appropriate pore size of the scaffolds. Thus, the proliferation of the cells on the scaffold of r-6%-0-2h was faster than that on the r-10%-1.0-1h.

4. Conclusion

In this work, an extrusion printable RSF-based pre-cured hydrogel was developed, employing high-molecular-weight RSF (HMWRSF) and urea. It was found that urea was certainly able to prolong the gelation process as a hydrogen bond disturber, because the crosslinker in the RSF-based physical hydrogel was a β-sheet domain/microcrystal, the molecular chains of which were organized by hydrogen bonding as the driving force. Therefore, there were enough microhydrogel-like domains in the pre-cured hydrogel to significantly contribute to its thixotropic property as well as self-supporting behavior. Indeed, the existence of the HMWRSF microhydrogel was demonstrated using the SEM images of the lyophilized hydrogel sponges at the early stage of gelation. As the formation of a β-sheet structure is a kinetic controlled process, no wonder that the preparation of those printable RSF-based hydrogels was highly related to a lot of factors such as the molecular weight of RSF, concentration or solid content of aqueous solution, amount of urea, gelation time and temperature, *etc.* On the other hand, 3D-bioprinted HMWRSF-based sponges displayed good mechanical properties and were able to be varied by formulation. Considering that urea involved could be completely washed out, the obtained HMWRSF-based sponge was expected to be a promising material for biomedical application.

Conflicts of interest

There are no conflicts to declare.

Acknowledgements

This work was supported by the National Natural Science Foundation of China (No. 21935002), the Ministry of Science and Technology of China (2020YFC2002804), the Shanghai Municipal Health Commission (201940170) and the Shanghai Natural Science Foundation (19ZR1407700).

References

1 J. K. Placone and A. J. Engler, *Adv. Healthcare Mater.*, 2018, **7**, e1701161.
2 S. C. Ligon, R. Liska, J. Stampfl, M. Gurr and R. Mulhaupt, *Chem. Rev.*, 2017, **117**, 10212–10290.
3 R. L. Truby and J. A. Lewis, *Nature*, 2016, **540**, 371–378.
4 S. Vijayavenkataraman, W. C. Yan, W. F. Lu, C. H. Wang and J. Y. H. Fuh, *Adv. Drug Delivery Rev.*, 2018, **132**, 296–332.
5 X. Li, B. Liu, B. Pei, J. Chen, D. Zhou, J. Peng, X. Zhang, W. Jia and T. Xu, *Chem. Rev.*, 2020, **120**, 10793–10833.
6 W. L. Ng, X. Huang, V. Shkolnikov, G. L. Goh, R. Suntornnond and W. Y. Yeong, *Int. J. Bioprint.*, 2022, **8**, 424.
7 P. Zhuang, W. L. Ng, J. An, C. K. Chua and L. P. Tan, *PLoS One*, 2019, **14**, e0216776.
8 S. Boularaoui, G. Al Hussein, K. A. Khan, N. Christoforou and C. Stefanini, *Bioprinting*, 2020, **20**, e0093.
9 Z. Fu, S. Naghieh, C. Xu, C. Wang, W. Sun and X. Chen, *Biofabrication*, 2021, **13**, 033001.
10 J. Zhang, Q. Hu, S. Wang, J. Tao and M. Gou, *Int. J. Bioprint.*, 2020, **6**, 242.
11 W. L. Ng, J. M. Lee, M. Zhou, Y. W. Chen, K. A. Lee, W. Y. Yeong and Y. F. Shen, *Biofabrication*, 2020, **12**, 022001.
12 W. Li, L. S. Mille, J. A. Robledo, T. Uribe, V. Huerta and Y. S. Zhang, *Adv. Healthcare Mater.*, 2020, **9**, e2000156.
13 H. Gudapati, M. Dey and I. Ozbolat, *Biomaterials*, 2016, **102**, 20–42.
14 S. Kawata, H.-B. Sun, T. Tanaka and K. Takada, *Nature*, 2001, **412**, 697–698.
15 V. F. Paz, M. Emons, K. Obata, A. Ovsianikov, S. Peterhänsel, K. Frenner, C. Reinhardt, B. Chichkov, U. Morgner and W. Osten, *J. Laser Appl.*, 2012, **24**, 042004.
16 S. V. Murphy and A. Atala, *Nat. Biotechnol.*, 2014, **32**, 773–785.
17 S. Bom, R. Ribeiro, H. M. Ribeiro, C. Santos and J. Marto, *Int. J. Pharm.*, 2022, **615**, 121506.
18 L. Valot, J. Martinez, A. Mehdi and G. Subra, *Chem. Soc. Rev.*, 2019, **48**, 4049–4086.
19 J. Gopinathan and I. Noh, *Biomater. Res.*, 2018, **22**, 11.
20 Z. Chen, Z. Li, J. Li, C. Liu, C. Lao, Y. Fu, C. Liu, Y. Li, P. Wang and Y. He, *J. Eur. Ceram. Soc.*, 2019, **39**, 661–687.
21 F. Kotz, K. Arnold, W. Bauer, D. Schild, N. Keller, K. Sachsenheimer, T. M. Nargang, C. Richter, D. Helmer and B. E. Rapp, *Nature*, 2017, **544**, 337–339.
22 K. Elhattab, S. B. Bhaduri and P. Sikder, *Polymers*, 2022, **14**, 1222.
23 Y. Sumbelli, S. Emir Diltemiz, M. G. Say, O. B. Unluer, A. Ersoz and R. Say, *Soft Matter*, 2021, **17**, 1008–1015.

24 S. A. Glukhova, V. S. Molchanov, Y. M. Chesnokov, B. V. Lokshin, E. P. Kharitonova and O. E. Philippova, *Carbohydr. Polym.*, 2022, **282**, 119106.
25 X. Mu, F. Agostinacchio, N. Xiang, Y. Pei, Y. Khan, C. Guo, P. Cebe, A. Motta and D. L. Kaplan, *Prog. Polym. Sci.*, 2021, **115**, 101375.
26 M. Wu, W. Yang, S. Chen, J. Yao, Z. Shao and X. Chen, *J. Mater. Chem. B*, 2018, **6**, 1179–1186.
27 S. Ling, Q. Wang, D. Zhang, Y. Zhang, X. Mu, D. L. Kaplan and M. J. Buehler, *Adv. Funct. Mater.*, 2018, **28**, 1705291.
28 W. Wang, Y. Liu, S. Wang, X. Fu, T. Zhao, X. Chen and Z. Shao, *ACS Appl. Mater. Interfaces*, 2020, **12**, 25353–25362.
29 Q. Dong, J. Cai, H. Wang, S. Chen, Y. Liu, J. Yao, Z. Shao and X. Chen, *Acta Biomater.*, 2020, **106**, 102–113.
30 Z. Mao, X. Bi, F. Ye, X. Shu, L. Sun, J. Guan, R. O. Ritchie and S. Wu, *ACS Biomater. Sci. Eng.*, 2020, **6**, 4512–4522.
31 S. Ghosh, S. T. Parker, X. Wang, D. L. Kaplan and J. A. Lewis, *Adv. Funct. Mater.*, 2008, **18**, 1883–1889.
32 S. Chawla, S. Midha, A. Sharma and S. Ghosh, *Adv. Healthcare Mater.*, 2018, **7**, e1701204.
33 M. J. Rodriguez, J. Brown, J. Giordano, S. J. Lin, F. G. Omenetto and D. L. Kaplan, *Biomaterials*, 2017, **117**, 105–115.
34 T. Dong, R. Mi, M. Wu, N. Zhong, X. Zhao, X. Chen and Z. Shao, *J. Mater. Chem. B*, 2019, **7**, 4328–4337.
35 X. Wang, J. A. Kluge, G. G. Leisk and D. L. Kaplan, *Biomaterials*, 2008, **29**, 1054–1064.
36 K. Luo, Y. Yang and Z. Shao, *Adv. Funct. Mater.*, 2016, **26**, 872–880.
37 Z. Gong, Y. Yang, Q. Ren, X. Chen and Z. Shao, *Soft Matter*, 2012, **8**, 2875–2883.
38 Y. Tao, K. Gu and Z.-z Shao, *Acta Polym. Sin.*, 2021, **52**, 158–165.
39 Z. Li, D. Li, Y. Chen and H. Cui, *Soft Matter*, 2018, **14**, 3858–3869.
40 S. Hartwig, J. Schwarz and S. Hecht, *J. Org. Chem.*, 2010, **75**, 772–782.
41 S. Paul and S. Paul, *J. Phys. Chem. B*, 2015, **119**, 10975–10988.
42 X. Chen, Z. Shao, N. S. Marinkovic, L. M. Miller, P. Zhou and M. R. Chance, *Biophys. Chem.*, 2001, **89**, 25–34.
43 D. Su, M. Yao, J. Liu, Y. Zhong, X. Chen and Z. Shao, *ACS Appl. Mater. Interfaces*, 2017, **9**, 17489–17498.
44 Z. Gong, L. Huang, Y. Yang, X. Chen and Z. Shao, *Chem. Commun.*, 2009, 7506–7508.
45 V. Karageorgiou and D. Kaplan, *Biomaterials*, 2005, **26**, 5474–5491.
46 W.-J. Li, C. T. Laurencin, E. J. Caterson, R. S. Tuan and F. K. Ko, *J. Biomed. Mater. Res.*, 2002, **60**, 613–621.
47 B. B. Seedholm, T. Takeda, M. Tsubuku and V. Wright, *Ann. Rheum. Dis.*, 1979, **38**, 307.
48 D. E. Shepherd and B. B. Seedhom, *Rheumatology*, 1999, **38**, 124–132.
49 Z. Cao, X. Chen, J. Yao, L. Huang and Z. Shao, *Soft Matter*, 2007, **3**, 910–915.
50 J. Jiang, C. Ai, Z. Zhan, P. Zhang, F. Wan, J. Chen, W. Hao, Y. Wang, J. Yao, Z. Shao, T. Chen, L. Zhou and S. Chen, *Artif. Organs*, 2016, **40**, 385–393.
51 X. Liu, Z. Toprakcioglu, A. J. Dear, A. Levin, F. S. Ruggeri, C. G. Taylor, M. Hu, J. R. Kumita, M. Andreasen, C. M. Dobson, U. Shimanovich and T. P. J. Knowles, *Macromol. Rapid Commun.*, 2019, **40**, e1800898.

